J Mater Sci (2023) 58:14879–14888

Metals & corrosion

Investigation of microstructure and deuterium retention in the reduced activation tungsten-steel brazed joint

J. Gurova[1,*], D. Bachurina[1], I. Kozlov[1], V. Bachurin[2], V. Efimov[1], O. Krutikova[1], A. Suchkov[1], N. Bobyr[3], A. Spitsyn[1,3], S. Simakin[2], and Y. Gasparyan[1]

[1] National Research Nuclear University MEPhI (Moscow Engineering Physics Institute), Kashirskoe Shosse 31, Moscow, Russia 115409
[2] Yaroslavl Branch, Valiev Institute of Physics and Technology of Russian Academy of Sciences, Yaroslavl, Russia 150007
[3] NRC "Kurchatov Institute", Ak. Kurchatov sq., 1, Moscow, Russia 123182

Received: 1 July 2023
Accepted: 7 September 2023
Published online: 22 September 2023

ABSTRACT

The combination of reduced-activation ferritic–martensitic steels (RAFM) and tungsten is suggested for plasma-facing components in future fusion reactors, but joining these materials is challenging. One promising method is a brazing technique that uses a Ta interlayer and a fully reduced activation brazing alloy, TiZr4Be. The initial microstructure of the Rusfer/TiZr4Be/Ta/TiZr4Be/W joint and transformations caused by exposure to D_2 gas at elevated temperatures and a pressure of 1 Pa were assessed using electron backscatter diffraction (EBSD), synchrotron X-ray diffraction analysis and secondary ion mass spectrometry. The joining layer was the main center of deuterium accumulation, but there were no changes in the microstructure after D_2 exposure at 300 °C. The total D retention after D_2 exposure at 600 °C was lower, but it was concentrated in the W/TiZr4Be/Ta seam, and the formation of an additional $ZrFe_2D_{2.66}$ phase was observed.

Introduction

Fusion energy promises to produce electricity with a high level of safety and low environmental impact. The favorable characteristics of fusion energy have been established as an alternative source of energy production on an industrial scale [1, 2]. The ITER fusion reactor is currently under construction and highlights many challenges that are associated with the design and selection of materials [3]. The next stage in the development of fusion energy sources will be reactors operating under more severe conditions, e.g., DEMO (DEMOnstration fusion reactor) [3–5]. Since the reactors will operate under more severe conditions than ITER, new approaches of the first wall are under development [6–10].

Tungsten is considered as a promising plasma facing material, with a reduced activation ferritic martensitic (RAFM) steel as a structural material [11] and therefore they should be joined. Methods to join tungsten

Handling Editor: P. Nash.

Address correspondence to E-mail: Violinarus@inbox.ru

https://doi.org/10.1007/s10853-023-08946-x

to steel could be divided into two main groups: brazing [12–16] and solid-state bonding [17–20]. Since the coefficient of thermal expansion (CTE) of tungsten and steel are drastically different, a compensating interlayer should be provided. As such an interlayer material with an intermediate CTE value can be used or a brazing alloy itself. When developing a method to join tungsten to steel one should follow the requirement of reduced activation [21]. Meanwhile just a few brazing approaches offer the usage of a fully reduced activation brazing alloy, e.g., Ti–Fe–Sn [22], Fe–Si–B [13] and Ti–Zr–Be [23]. The least research was carried out by our team and was extensively investigated so far, this joint Rusfer/TiZr4Be/Ta/TiZr4Be/W was the object of this article.

Although there is a number of investigations aimed at the tungsten/steel joining, only a few of them presented the results on the behavior of the joints in hydrogen isotopes environment. Wang et al. [24] showed that the W/Ti/(91 grade steel) diffusion bonded joint exposed to 200–1000 Pa remains integrated. When the joint was exposed at 0.1 MPa, it failed. We investigated deuterium retention in the Rusfer/TiZr4Be/Ta/TiZr4Be/W joint [25]. It was shown that the joint withstands the normal First Wall DEMO exposure conditions, while the deuterium amount in the intermediate layer grows substantially with the increase of the surrounding deuterium pressure. This paper presents a more detailed analysis of deuterium distribution and microstructure transformation in the joint after deuterium gas exposure using several technics. For a better understanding of the microstructure of the obtained compounds, this article presents the results of EBSD (Electron backscatter diffraction), SynXRD (synchrotron X-Ray diffraction analysis) and SIMS (the secondary ion mass spectrometry) and other studies, since the TDS analysis itself provides only general information about the temperatures at which deuterium is released and how much of it is captured in the integral.

Experimental details

We used vacuum brazed joints Rusfer/TiZr4Be/Ta/TiZr4Be/W, where W—ITER grade tungsten, Rusfer—RAFM Rusfer EK-181, Ta—pure tantalum interlayer, which was used to suppress the mismatch of CTE between W and Rusfer, TiZr4Be—rapidly solidified into ribbon alloy of the following composition 48Ti–48Zr–4Be wt%. W and Rusfer were in the form of cubes with the dimensions of $5 \times 5 \times 3$ mm^3 (width × length × thickness). The Ta interlayer with the dimensions of $5 \times 5 \times 0.18$ mm^3. The TiZr4Be brazing with a thickness of 70 μm alloy was used. The brazing procedure included thermal heat treatment at 1100 °C for 1 h and aging at 720 °C for 3 h (see [23] for details).

Deuterium gas (D_2) exposure was performed at the pressure of 1 Pa for 2 h at two different temperatures: 300 °C and 600 °C (see [25] for details).

The microstructure of the samples was analyzed by scanning electron microscope (SEM) TESCAN CLARA equipped with EBSD Oxford Instruments Nordlys Nano and EDS Oxford Instruments Ultim MAX 100. Prior to the analysis, the samples were grinded and polished with subsequent ion etching by Technoorg Linda SEMPrep2.

SynXRD was applied to get deeper understanding of the microstructure. Recording of the XRD pattern was conducted at the Kurchatov Synchrotron Radiation Source with the wavelength of 0.74 Å. The procedure was previously presented elsewhere [25, 26]. Two spectra were recorded for each brazed seam in slightly different positions in order to cover all phases.

SIMS method using the TOF. SIMS^5 facility provided an additional information about deuterium distribution in the sample. The analysis was carried out in several modes with registration of both positive and negative secondary ions. A beam of Bi_3^+ ions with the energy of 25 keV was used as an analyzing beam. The probing beam was unfolded into a raster with a size of 500×500 μm^2. Ion etching of the analyzed surface, aimed at its cleaning and chemical modification, was carried out with Cs^+ ions (in the case of obtaining an ion microscopic image in negative secondary ions) and O_2^+ (in positive secondary ions) with an energy of 2 keV. Accumulation of the signal was carried out by frames with a discreteness of 128×128 or 256×256 points. The entire mass spectrum was stored in the range $0 \div 430$ a.m.u. for each point of the frame.

As-joined microstructure

Figure 1 shows the microstructures of two composing seams: Rusfer/TiZr4Be/Ta—a and Ta/TiZr4Be/W—b and c. Comparing the microstructure of Ta/TiZr4Be/W in [23] and [25], we found the formation of different phases in this seam due to the contact of the melts from Rusfer/TiZr4Be/Ta and Ta/TiZr4Be/W seams.

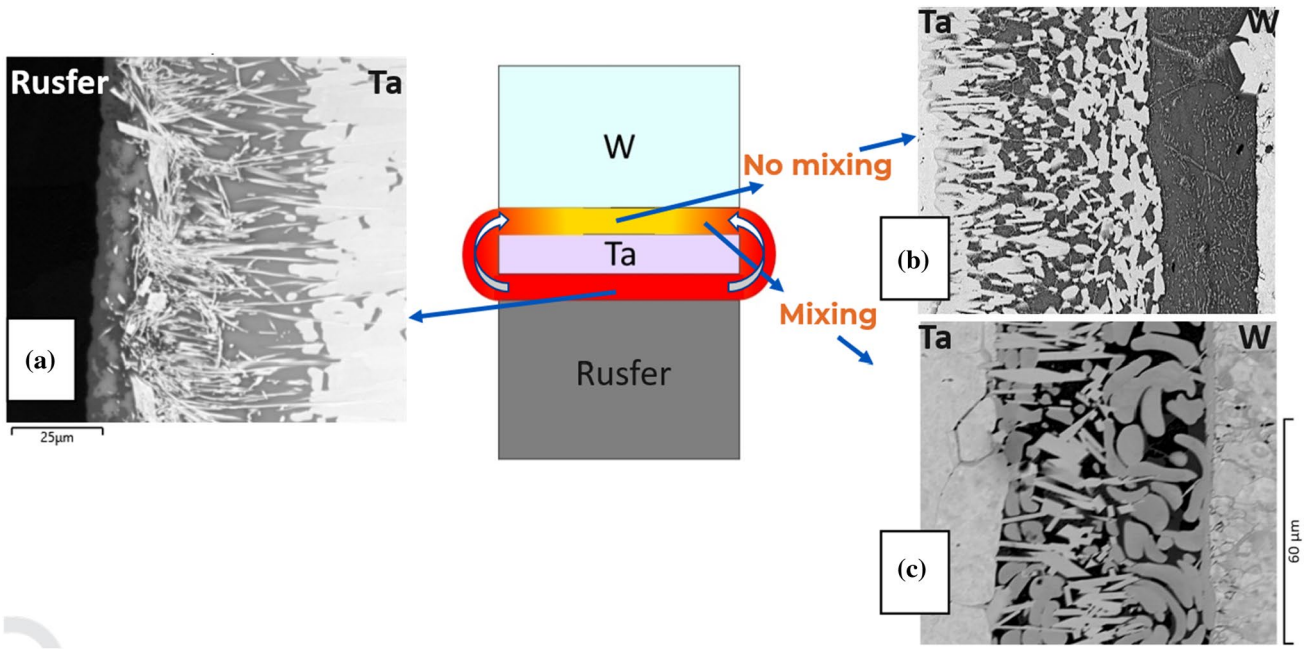

Figure 1 Microstructure of Rusfer/TiZr4Be/Ta/TiZr4Be/W brazed joint and schematic representation of the mixing effect due to the contact of the melts from Rusfer/TiZr4Be/Ta and Ta/TiZr4Be/W seams.

This phenomenon schematically presented in Fig. 1. If the melts of Rusfer/TiZr4Be/Ta and Ta/TiZr4Be/W do not contact each other (*no mixing* of the melts occurs), the microstructure presented in Fig. 1b forms, on the other hand if the melts contact each other (*mixing* of the melts occurs)—Fig. 1c. At the same time, the microstructure similar to Rusfer/TiZr4Be/Ta seam is formed in the fillet region.

During the brazing process, the dissolution of base materials is a common phenomenon that is typically referred to as "erosion." In our case, the steel is more prone to dissolve in molten TiZr4Be due to the existence of eutectics between Fe and the components of the filler alloy. Simultaneously, TiZr4Be exhibited a high wetting ability at the bonding temperature. These two factors led to the contact of two melts: one with a high concentration of Fe and C atoms (at the steel side), and another with a low concentration of the same elements (tungsten side). As a result, a gradient of concentration occurred, leading to the transport of atoms from the Rusfer/Ta side toward the Ta/W side. Since the tantalum buffer layer had the same dimensions as the base materials, there were no obstacles to the mixing process. Using a larger buffer layer and less brazing alloy could help avoid this phenomenon. However, we do not consider it a negative factor and instead aim to provide insights into the microstructural differences.

Microstructure of Rusfer/TiZr4Be/Ta seam

The Rusfer/TiZr4Be/Ta seam was investigated earlier in [23] by EBSD. We found out that the seam consists of the following phases: bcc-Fe (αFe), ZrC, Ta_2Be, bcc-Ta (αTa) and $ZrFe_2$ phases. EBSD is a local microanalysis, but XRD and especially XRD with synchrotron irradiation allows to define fine phases within the bulk sample. Hence, we have refined the microstructure of the Rusfer/TiZr4Be/Ta brazed joint by SynXRD in this work.

Figure 2 shows the SynXRD pattern of the Rusfer/TiZr4Be/Ta joint. The presence of the αFe phase was established and confirmed. In addition to αFe, the γFe phase was identified in the pattern, which is responsible for the retained austenite. Analyzing the SynXRD spectra, the presence of ZrC and $ZrFe_2$ was also established. Additionally, we found TiC carbide. It can be assumed that carbides are formed inside the ferritic grains in the form of small precipitates, similarly to the formation of TiC in brazed joint obtained by Cu-Ti brazing alloys [26]. Hence, SynXRD supported EBSD results and establish the presence of TiC phase.

Taking into account dissolution of the elements according to EDS maps, one can suggest the following composition of the Rusfer/TiZr4Be/Ta seam: αFe, γFe, Ta_2Be, ZrC, $(Zr,Ti)_2(Fe,Cr,Ta)$, α(Ta,Ti), TiC.

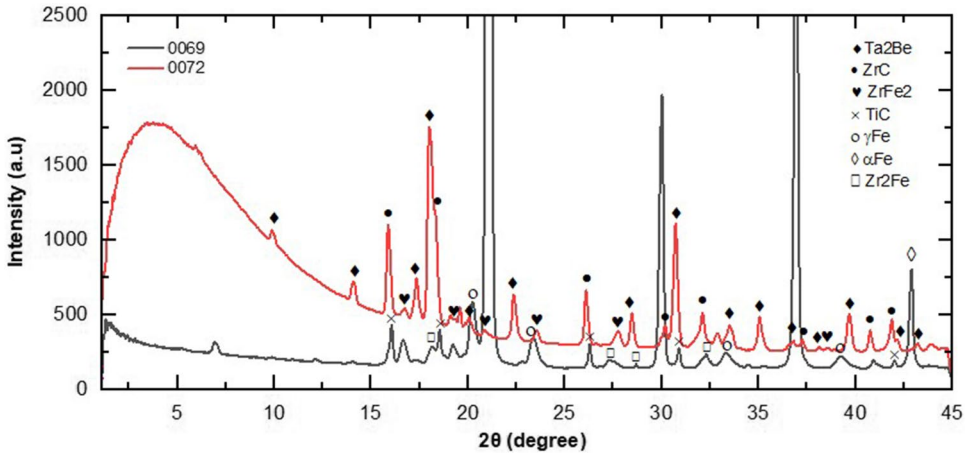

Figure 2 SynXRD spectra of the Rusfer/TiZr4Be/Ta seam.

Microstructure of Ta/TiZr4Be/W seam

According to EBSD [23], it was found that the brazed seam with *no mixing* consists of αTa, αW, Ta_2Be, βTa, solid solution based on bcc-Ti (β(Ti, Zr, Ta)), ZrC. All these phases were found by SynXRD (Fig. 3) as well. Additionally, we found other phases with the figure-of-merit no less than 0.77: TiC, TaC and $Be_{12}Ti$. The presence of carbides in this seam shows that there was still a contact of the melts, but the mixing is not intense and no Fe-containing phases form. So Ta/TiZr4Be/W joint with *no mixing* consists of: αTa, αW, Ta_2Be, βTa, β(Ti, Zr, Ta), ZrC, TiC, TaC and $Be_{12}Ti$.

In the case of *mixing*, the microstructure of the Ta/TiZr4Be/W seam looks very different (Fig. 1c). EBSD, EDS maps and SynXRD spectra for this case are given in Figs. 4 and 5.

By EBSD, we found following components: αTa, αW, Ta_2Be, $ZrFe_2$ and ZrC. αTa grains formed in the initial Ta interlayer in the seam. In the seam, αTa dissolves titanium, zirconium and iron (52Ta–36.5Ti–6.5Zr–3W–2Fe at%), which can be written as α(Ta, Ti, Zr, W, Fe). The morphology of the Ta_2Be phase is different from that observed in the Ta/TiZr4Be/W brazed joint *without mixing* (Fig. 1b). The amount of ZrC phase in this joint is lower compared to the brazed joint without *mixing*.

By EDS analysis composition of $ZrFe_2$ measured as: 51Ti–31Zr–14Ta–3Fe at%, hence it can be rewritten as as $(Ti, Zr)(Ta, Fe)_2$. Along αW grain boundaries, α(Ta, Ti, Zr, W, Fe) and $(Ti, Zr)(Ta, Fe)_2$ phases were found. The EDS map shows that the $(Ti, Zr)(Ta, Fe)_2$ phase could also form at the α(Ta, Ti, Zr, W, Fe)/αW interface.

Additionally to EBSD, we found other phases by SynXRD: TiC, TaC and a bcc structure which can correlate to $TiZrC_2$. Since the carbides where not found by EBSD, we can conclude that they formed

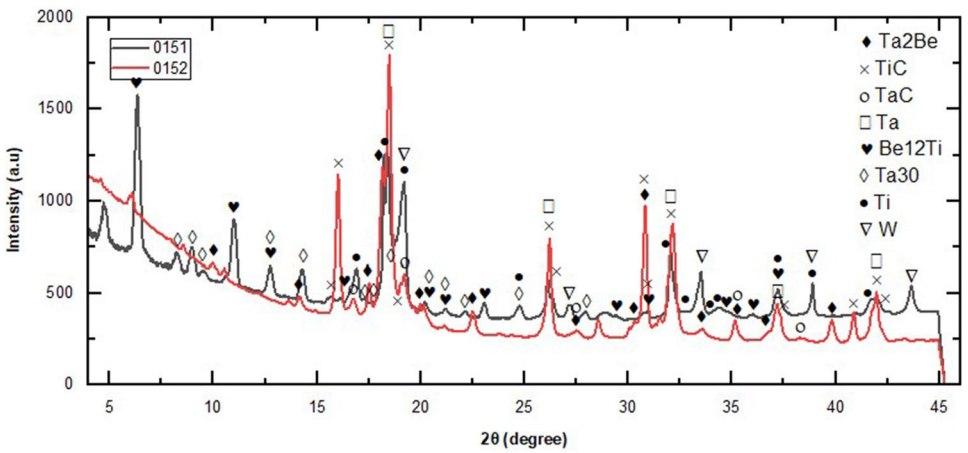

Figure 3 SynXRD spectra of Ta/TiZr4Be/W seam with *no mixing* between two composing seams of Rusfer/TiZr4Be/Ta/TiZr4Be/W brazed joint.

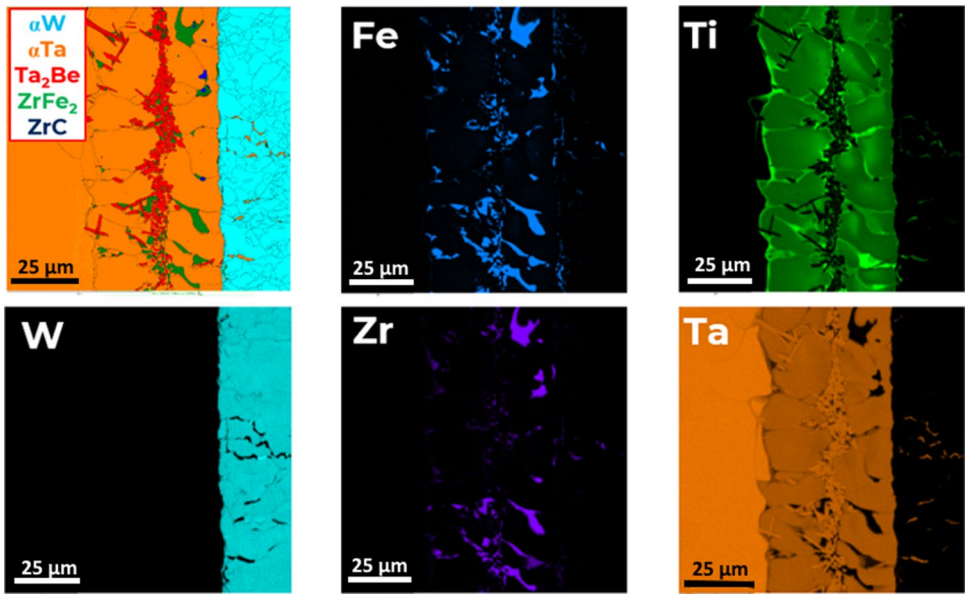

Figure 4 EBSD phase map and EDS maps of Ta/TiZr4Be/W seam with *mixing* between two composing seams of Rusfer/TiZr4Be/Ta/TiZr4Be/W brazed joint.

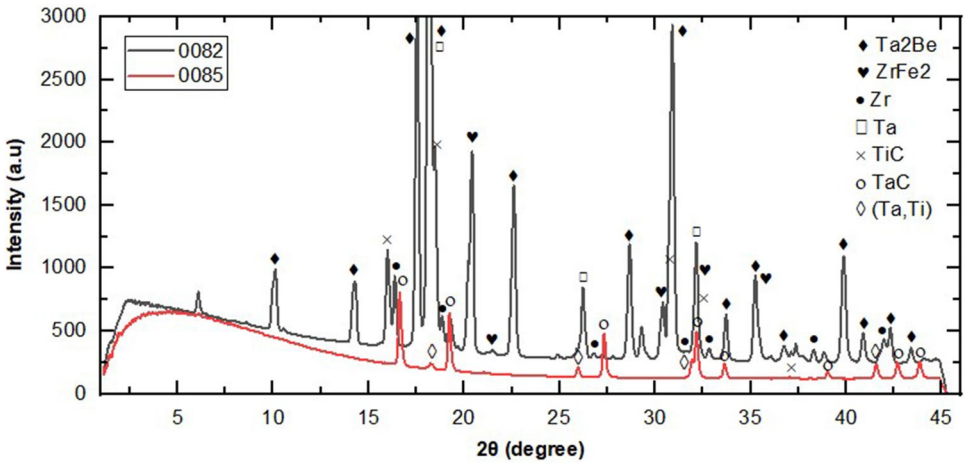

Figure 5 SynXRD spectra of Ta/TiZr4Be/W seam with *mixing* between two composing seams of Rusfer/TiZr4Be/Ta/TiZr4Be/W brazed joint.

in a very fine size. At the same time, unidentified peaks remained on the diffraction spectrum. Nevertheless, we can confirm that the brazed seam Ta/TiZr4Be/W with *mixing* consists of at least: αTa, αW, α(Ta,Ti,Zr,W,Fe), Ta_2Be, (Ti,Zr)$(Ta,Fe)_2$, ZrC, TaC, TiC, $TiZrC_2$.

Concluding the above results, we proved that the Ta/TiZr4Be/W seam may have different microstructure depending on the mixing of the melts from both seams (Rusfer/TiZr4Be/Ta and Ta/TiZr4Be/W):

- *no mixing*: αTa, αW, Ta_2Be, βTa, β(Ti, Zr, Ta), ZrC, TiC, TaC and $Be_{12}Ti$;
- *mixing*: αTa, αW, α(Ta,Ti,Zr,W,Fe), Ta_2Be, (Ti,Zr)$(Ta,Fe)_2$, ZrC, TaC, TiC, $TiZrC_2$.

In the subsequent stages of our work, we have planned to conduct tests aimed at revealing the influence of each phase on the mechanical performance of the joint.

Microstructure after deuterium exposure

SynXRD of the joint after deuterium retention was carried out as well. Finalized results of the analysis are collected in Table 1. We found no hydrides in the Rusfer/TiZr4Be/Ta joint and in the Ta/TiZr4Be/W joint with no mixing. Hydrides were found only in the Ta/TiZr4Be/W joint *with mixing* after deuterium exposure at 600 °C: $ZrFe_2D_{2.66}$ (ICDD #01-072-6471). Figure 6

Table 1 Phase composition of Rusfer/TiZr4Be/Ta/ TiZr4Be/W in the as-joined state and after deuterium exposure

	As-joined	300 °C, D_2	600 °C, D_2
Rusfer/TiZr4Be/Ta	αFe, γFe, Ta_2Be, ZrC, $(Zr,Ti)_2(Fe,Cr,Ta)$, α(Ta,Ti), TiC	No change	No change
Ta/TiZr4Be/W no mixing	αTa, αW, Ta_2Be, βTa, β(Ti, Zr, Ta), ZrC, TiC, TaC and $Be_{12}Ti$	No change	No change
Ta/TiZr4Be/W mixing	αTa, αW, α(Ta,Ti,Zr,W,Fe), Ta_2Be, (Ti,Zr)$(Ta,Fe)_2$, ZrC, TaC, TiC, $TiZrC_2$	No change	As-joined + $ZrFe_2D_{2.66}$
D retention, 10^{22} D/m^2 (TDS data) Adapted with permission from reference [25]. Copyright [2022], [J. Nucl. Mater]	–	20 ± 4	2.8 ± 0.5
Shear strength, MPa Adapted with permission from reference [25]. Copyright [2022], [J. Nucl. Mater]	118 ± 28	80 ± 16	80 ± 30

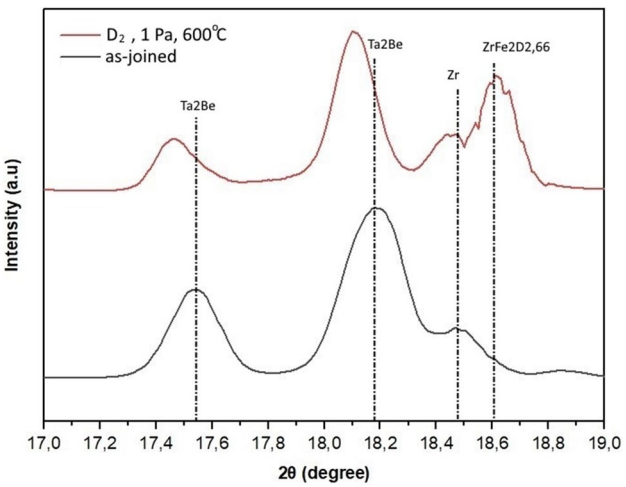

Figure 6 Main intensities of Ta/TiZr4Be/W SynXRD with *mixing* in as-joined and exposed to deuterium state.

shows SynXRD spectra between 17° and 19° of Ta/TiZr4Be/W with *mixing* in as-joined and exposed state, the spectra are shown for the main peaks pointing out formation of a new peak for $ZrFe_2D_{2.66.}$ In addition, a shift of the peaks of the Ta_2Be phase is noted, which indicates a change in the lattice parameter. At this stage, it is not possible to reliably determine the cause of the shift, but it can be assumed that the formation of the $ZrFe_2D_{2.66}$ phase has led to the deformation in the neighboring phases. The fact that this phase formed at 600 °C coincides with the previous research where a Zr-based phase of a round outline was formed [25].

Figure 7 shows SIMS elemental maps and deuterium profiles in the Rusfer/TiZr4Be/Ta/TiZr4Be/W joint, obtained by SIMS and SEM: a, c—exposure at 300° C during 50 h at 1 Pa; b, d—exposure at 600 °C during 50 h at 1 Pa.

The maximum concentration of deuterium is observed in the brazed seam. In the case of exposure at 300 °C (Fig. 7a, c), deuterium is found both in the W/TiZr4Be/Ta seam and in the Ta/TiZr4Be/Rusfer seam. At the same time, in the case of exposure at 600 °C (Fig. 7b, d), deuterium is found mainly in the W/TiZr4Be/Ta seam.

In the sample exposed at 300 °C (Fig. 7a, c), deuterium is clearly observed in tantalum, but its amount is several times less than in the brazed joints. The solubility of hydrogen in tantalum is less than in the alloying elements of the brazing alloy (titanium and zirconium). An increased concentration of deuterium is found in the area of elongated β(Ta, Ti) grains in the Ta/TiZr4Be/Rusfer brazed seam. The maximum values of deuterium coincides with a high concentration of the Ta_2Be phase; therefore, it can be concluded that the formation of the Ta_2Be phase contributes to the increase in the capture at this temperature.

In the sample exposed at 600 °C (Fig. 7b, d), deuterium retention is predominantly carried out in the W/TiZr4Be/Ta brazed seam; in the brazed seam Ta/TiZr4Be/Rusfer a slight increase in the deuterium concentration is observed in elongated β(Ta, Ti) grains. In general, this indicates a significant difference in the structure of the two seams and a different ability to retain hydrogen. The concentration maximum coincides with the β(Ti, Zr, Ta) phase in the W/TiZr4Be/Ta seam. Figure 7 b, d shows the profile of deuterium, which was obtained in the area of the brazed seam, where this phase is clearly separated. With a shift from β(Ti, Zr, Ta) to Ta, the

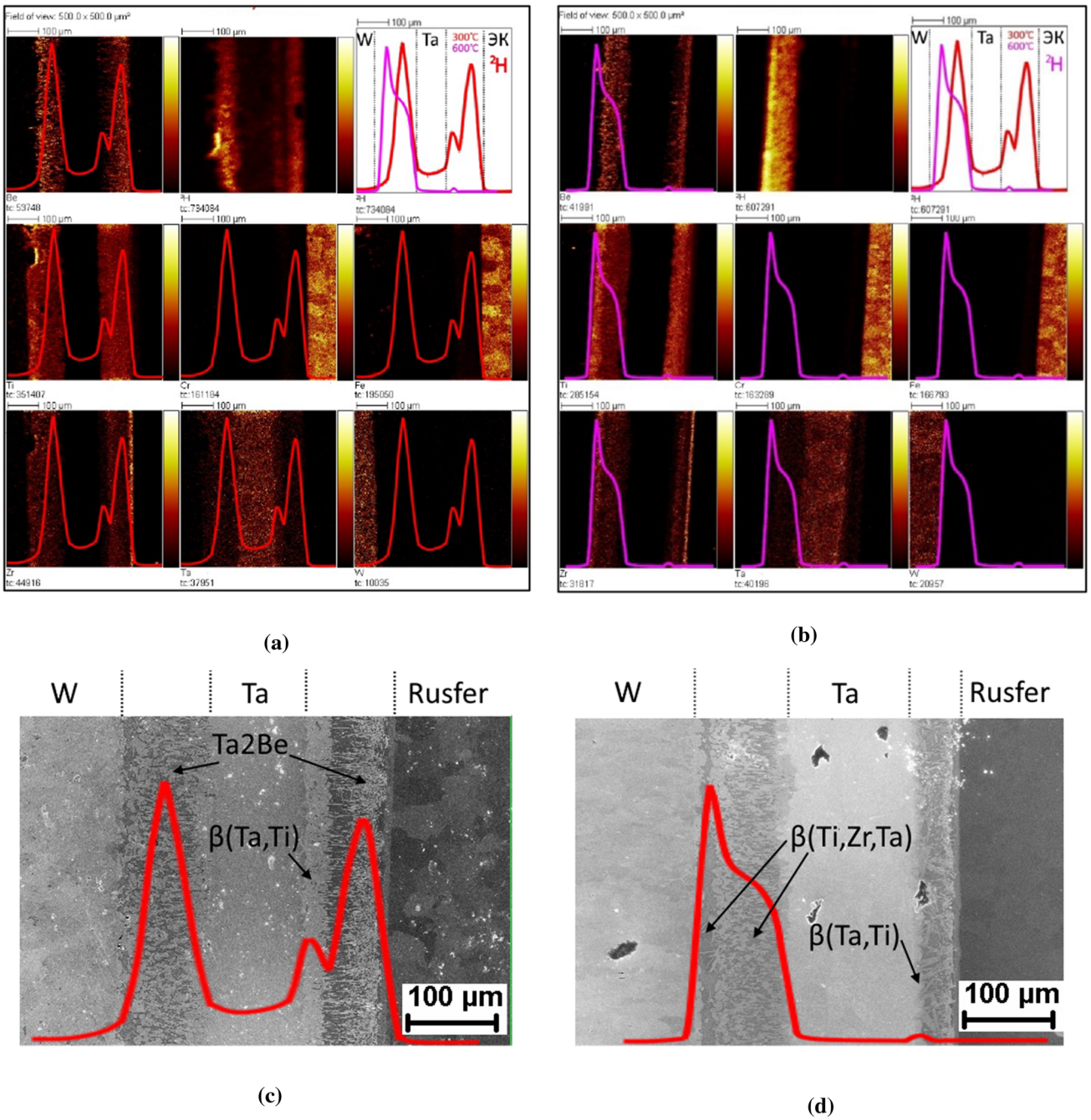

Figure 7 SIMS elemental maps and deuterium profiles of the brazed seams exposed to deuterium.

deuterium concentration decreases, but does not drop to zero. This is primarily due to the fact that β(Ti, Zr, Ta) is also present in this region, and it is also here that the $ZrFe_2D_{2.66}$ hydride can be formed, which was revealed using Syn-XRD (Table 1). Thus, it can be assumed that at 600 °C the retention of deuterium in the Ta_2Be phase is significantly reduced, and the capture of deuterium occurs mainly due to β(Ti, Zr, Ta) in the W/TiZr4Be/Ta seam, as well as due to the $ZrFe_2D_{2.66}$ phase.

Discussions

Although the formation of a significant amount of hydrides is not observed, previous studies have demonstrated that these joints capture deuterium in quantities of $(20 \pm 4) \times 10^{22}$ D/m^2 at 300 °C and $(2.8 \pm 0.5) \times 10^{22}$ D/m^2 at 600 °C [25]. The average shear strength values of these samples are the same; however, the deviation of the sample exposed to 600 °C was larger, possibly due to the inhomogeneous distribution of the $ZrFe_2D_{2.66}$ phase. In order to gain a deeper understanding of the lower retention value at 600 °C, we conducted SIMS analysis to assess the path of deuterium retention.

Firstly, the lower level of retention in the sample exposed to 600 °C is attributed to the desorption that already occurs at this temperature [25]. Clearly, as the temperature increases, the mobility of deuterium also increases. Conversely, deuterium stops being retained in trapping centers with low binding energy. Upon comparing the images provided by SIMS, we deduced that this is predominantly due to desorption from Ta_2Be. Additionally, we can assert that Ta_2Be primarily influences retention at 300 °C, while β(Ti, Zr, Ta) becomes significant at 600 °C. The $ZrFe_2D_{2.66}$ phase should also play an important role at 600 °C; however, at the available resolution, we were unable to pinpoint the exact locations of this phase. We assume that a minimum of $(30 \pm 6) \times 10^{22}$ D/m^2 is required to resolve this phase by SEM, as it was easily found at this retention level in previous research [25].

Drawing a definitive conclusion regarding why deuterium exhibits stronger segregation in certain phases than in others is complex, as the brazing process is multicomponent. Evaluating the processes occurring within it from a thermodynamic perspective proves challenging. However, one of the factors influencing the segregation process to a greater extent in certain phases than in others could be the binding energy value.

Conclusions

Brazing W to RAFM Rusfer steel using the 48Ti–48Zr–4Be wt% alloy and the Ta interlayer seems to be a prospective solution for future fusion reactors. Meanwhile hydrogen isotopes retention may play a drastic role, so the deep understanding of the brazed seams microstructure and deuterium retention were assessed.

The analysis of the microstructure of the brazed seams using EBSD, EDS and SynXRD techniques revealed the presence of various phases in the Rusfer/TiZr4Be/Ta brazed seam. The Ta/TiZr4Be/W brazed seam, on the other hand, tended to form a different microstructure depending on whether the melts mix between the Rusfer/TiZr4Be/Ta and Ta/TiZr4Be/W seams or not.

The SIMS analysis demonstrated that the joint accumulates deuterium through both the Rusfer/TiZr4Be/Ta and Ta/TiZr4Be/W seams at 300 °C, but at 600 °C the major part of deuterium is concentrated in the Ta/TiZr4Be/W seam.

No hydrides were identified after exposure at 300 °C. In this case, the Ta_2Be phase is suggested to be main deuterium trapping centers, from where deuterium desorbs at 600 °C. However, β(Ti, Zr, Ta) and the newly formed $ZrFe_2D_{2.66}$ phase may accumulate a substantial deuterium amount even at 600 °C. Formation of hydrides can potentially initiate a degradation of mechanical properties, which was not observed in our time scales. Therefore, more accurate investigations are needed to determine the operation window of these systems.

Acknowledgements

Authors acknowledge Tescan Russia for the microstructural analysis. SIMS measurements were carried out and using equipment of the Center for Collective Use Diagnostics of Microstructures and Nanostructures.

Author contributions

The combination of reduced-activation ferritic–martensitic steels (RAFM) and tungsten are suggested for plasma facing components in future fusion reactors, but joining of these materials is challenging. One of promising ways is a brazing technique using a Ta interlayer and a fully reduced activation brazing alloy TiZr4Be. The initial microstructure of the Rusfer/TiZr4Be/Ta/TiZr4Be/W joint and transformations caused by exposure in D2 gas at elevated temperatures and the pressure of 1 Pa were assessed using electron backscatter diffraction (EBSD), synchrotron

X-ray diffraction (SynXRD) analysis and Secondary Ion Mass Spectrometry (SIMS). The joining layer was the main center of deuterium accumulation, but there were no changes in the microstructure after D2 exposure at 300 °C. The total D retention after D2 exposure at 600 °C was lower, but it was concentrated in the W/TiZr4Be/Ta seam and formation of an additional ZrFe2D2.66 phase was observed.

Funding

Sample characterization using the Synchrotron was done with the support of the Ministry of Science and Higher Education of the Russian Federation (Agreement No. 075-15-2021-1352).

Data and code availability

Data are available from the authors on request.

Declarations

Conflict of interest The authors declare that they have no known competing financial interests or personal relationships that could have appeared to influence the work reported in this paper.

References

[1] Maisonnier D (2005) Final report of the European fusion power plant conceptual study (PPCS), EFDA(05)-27/4.10, vol 1.

[2] Najmabadi F, Abdou A, Bromberg L, Brown T, Chan VC, Chu MC, Dahlgren F, El-Guebaly L, Heitzenroeder P, Henderson D, St John HE, Kessel CE, Lao LL, Longhurst GR, Malang S, Mau TK, Merrill BJ, Miller RL, Mogahed E, Moore RL, Petrie T, Petti DA, Politzer P, Raffray AR, Steiner D, Sviatoslavsky I, Synder P, Syaebler GM, Turnbull AD, Tillack MS, Waganer LM, Wang X, West P, Wilson P (2006) The ARIES-AT advanced tokamak, advanced technology fusion power plant. Fusion Eng Des 80:3–23. https://doi.org/10.1016/j.fusengdes.2005.11.003

[3] Maisonnier D, Campbell D, Cook I, Di Pace L, Giancarli L, Hayward J, Li Puma A, Medrano M, Norajitra P, Roccella M, Sardain P, Tran MQ, Ward D (2007) Power plant conceptual studies in Europe. Nucl Fusion 47:1524–1532. https://doi.org/10.1088/0029-5515/47/11/014

[4] Yamada H, Kasada R, Ozaki A, Sakamoto R, Sakamoto Y, Takenaga H, Tanaka T, Tanigawa H, Okano K, Tobita K, Kaneko O, Ushigusa K (2016) Development of strategic establishment of technology bases for a fusion DEMO reactor in Japan. J Fusion Energy 35:4–26. https://doi.org/10.1007/s10894-015-0018-1

[5] Kim K, Im K, Kim HC, Oh S, Park JS, Kwon S, Lee YS, Yeom JH, Lee C, Lee GS, Neilson G, Kessel C, Brown T, Titus P, Mikkelsen D, Zhai Y (2015) Design concept of K-DEMO for near-term implementation. Nucl Fusion. https://doi.org/10.1088/0029-5515/55/5/053027

[6] Forest L, Aktaa J, Boccaccini LV, Emmerich T, Eugenghidersa B, Fondant G, Froio A, Puma AL, Namburi H, Neuberger H, Rey J, Savoldi L, Sornin D, Vala L (2020) Status of the EU DEMO breeding blanket manufacturing R&D activities. Fusion Eng Des 152:111420. https://doi.org/10.1016/j.fusengdes.2019.111420

[7] Del Nevo A, Arena P, Caruso G, Chiovaro P, Di Maio PA, Eboli M, Edemetti F, Forgione N, Forte R, Froio A, Giannetti F, Di Gironimo G, Jiang K, Liu S, Moro F, Mozzillo R, Savoldi L, Tarallo A, Tarantino M, Tassone A, Utili M, Villari R, Zanino R, Martelli E (2019) Recent progress in developing a feasible and integrated conceptual design of the WCLL BB in EUROfusion project. Fusion Eng Des 146:1805–1809. https://doi.org/10.1016/j.fusengdes.2019.03.040

[8] Tassone A, Del Nevo A, Arena P, Bongiovi G, Caruso G, Di Maio PA, Di Gironimo G, Eboli M, Forgione N, Forte R, Giannetti F, Mariano G, Martelli E, Moro F, Mozzillo R, Tarallo A, Villari R (2018) Recent progress in the WCLL breeding blanket design for the DEMO fusion reactor. IEEE Trans Plasma Sci 46:1446–1457. https://doi.org/10.1109/TPS.2017.2786046

[9] Martelli E, Giannetti F, Caruso G, Tarallo A, Polidori M, Barucca L, Del Nevo A (2018) Study of EU DEMO WCLL breeding blanket and primary heat transfer system integration. Fusion Eng Des 136:828–833. https://doi.org/10.1016/j.fusengdes.2018.04.016

[10] Kamenický R, Domalapally PK, Arnoult X (2018) Thermomechanical stress analysis of the water cooled DEMO first wall mock-up components. Fusion Eng Des 136:1618–1623. https://doi.org/10.1016/j.fusengdes.2018.05.072

[11] Igitkhanov Y, Bazylev B, Landman I, Boccaccini L (2013) Applicability of tungsten/EUROFER blanket module for the DEMO first wall. J Nucl Mater 438:S440–S444. https://doi.org/10.1016/j.jnucmat.2013.01.089

[12] de Prado J, Sánchez M, Arbizu G, Ureña A (2020) In-situ SEM fracture analysis of W-Eurofer brazed joints under

three-point bending test configuration. Metall Mater Trans A Phys Metall Mater Sci 51:3488–3496. https://doi.org/10.1007/s11661-020-05762-9

[13] Wang J, Lian Y, Feng F, Liu X, Chen Z, Wang Y, Qiang J, Wei M (2021) Tungsten/reduced activation ferritic–martensitic steel joints made with an Fe–Si–B amorphous filler. Mater Sci Technol (United Kingdom). https://doi.org/10.1080/02670836.2021.1987703

[14] Bachurina D, Vorkel V, Suchkov A, Gurova J, Ivannikov A, Penyaz M, Fedotov I, Sevryukov O, Kalin B (2021) Overview of the mechanical properties of tungsten/steel brazed joints for the demo fusion reactor. Metals (Basel) 11:1–11. https://doi.org/10.3390/met11020209

[15] de Prado J, Sánchez M, Ruiz A, Ureña A (2020) Effect of brazing temperature, filler thickness and post brazing heat treatment on the microstructure and mechanical properties of W-Eurofer joints brazed with Cu interlayers. J Nucl Mater. https://doi.org/10.1016/j.jnucmat.2020.152117

[16] Peng L, Mao Y, Zhang Y, Xi L, Deng Q, Wang G (2018) Microstructural and mechanical characterizations of W/CuCrZr and W/steel joints brazed with Cu-22TiH_2 filler. J Mater Process Tech 254:346–352. https://doi.org/10.1016/j.jmatprotec.2017.11.056

[17] Zhu W, Liu W, Ma Y, Cai Q, Wang J, Duan Y (2021) Microstructural characteristics, mechanical properties and interfacial formation mechanism of tungsten alloy/steel composite structure fabricated by HIP co-sintering. Mater Des 211:110127. https://doi.org/10.1016/j.matdes.2021.110127

[18] Huang P, Wang Y, Peng H, Chen J, Wang P (2020) Diffusion bonding W and RAFM-steel with an Fe interlayer by hot isostatic pressing. Fusion Eng Des. https://doi.org/10.1016/j.fusengdes.2020.111796

[19] Cai Q, Liu W, Ma Y, Zhu W, Pang X (2018) Effect of joining temperature on the microstructure and strength of W–steel HIP joints with Ti/Cu composite interlayer. J Nucl Mater 507:198–207. https://doi.org/10.1016/j.jnucmat.2018.05.004

[20] Basuki WW, Aktaa J (2015) Process optimization for diffusion bonding of tungsten with EUROFER97 using a vanadium interlayer. J Nucl Mater 459:217–224. https://doi.org/10.1016/j.jnucmat.2015.01.033

[21] Gilbert MR, Sublet J-C, Forrest RA (2015) Handbook of activation, transmutation, and radiation damage properties of the elements simulated using FISPACT-II & TENDL-2014; Magnetic Fusion Plants, Ccfe-R(15)26. pp 1–696. http://www.ccfe.ac.uk/assets/documents/easy/CCFE-R(15)26.pdf.

[22] Zhu W, Qiang J, Wang Y, Sun J, Wang J, Lian Y, Feng F, Liu X (2017) A Ti–Fe–Sn thin film assembly for joining tungsten and reduced activation ferritic–martensitic steels. Mater Des 125:55–61. https://doi.org/10.1016/j.matdes.2017.03.060

[23] Bachurina D, Suchkov A, Gurova J, Kliucharev V, Vorkel V, Savelyev M, Somov P, Sevryukov O (2021) Brazing tungsten/tantalum/RAFM steel joint for DEMO by fully reduced activation brazing alloy 48Ti–48Zr–4Be. Metals (Basel). https://doi.org/10.3390/met11091417

[24] Wang JC, Huang J, Sun H, Gao X, Wang W, Li Q, Xie C, Wang X, Chen Z, Gao Q, Liu S, Luo GN, Li J (2019) Effect of deuterium on bonding quality of W/Ti/Steel HIP joints in first wall application. Fusion Eng Des 138:313–320. https://doi.org/10.1016/j.fusengdes.2018.12.010

[25] Gasparyan Y, Bachurina D, Efimov V, Gurova J, Podolyako F, Sergeev N, Sorokin I, Suchkov A, Bobyr N, Kozlov I, Kulikova E, Spitsyn A (2022) Deuterium retention in the elements of plasma facing components for the DEMO first wall. J Nucl Mater 567:153837. https://doi.org/10.1016/j.jnucmat.2022.153837

[26] Bachurina D, Suchkov A, Gurova J, Savelyev M, Dzhumaev P, Kozlov I, Svetogorov R, Leont'eva-Smirnova M, Sevryukov O (2020) Joining tungsten with steel for DEMO: simultaneous brazing by Cu–Ti amorphous foils and heat treatment. Fusion Eng Des 162:112099. https://doi.org/10.1016/j.fusengdes.2020.112099